Journal of Water Process Engineering 53 (2023) 103595

Contents lists available at ScienceDirect

Journal of Water Process Engineering

journal homepage: www.elsevier.com/locate/jwpe

Proof-of-concept approach to assess the impact of thermal disinfection on biofilm structure in hot water networks

Ana Rosa Silva, Diogo A.C. Narciso, Luciana C. Gomes, F.G. Martins, Luis F. Melo, Ana Pereira *

LEPABE - Laboratory for Process Engineering, Environment, Biotechnology and Energy, Faculty of Engineering, University of Porto, Rua Dr. Roberto Frias, 4200-465 Porto, Portugal
ALiCE - Associate Laboratory in Chemical Engineering, Faculty of Engineering, University of Porto, Rua Dr. Roberto Frias, 4200-465 Porto, Portugal

ARTICLE INFO

Keywords:
Biofilm regrowth
Biofilm structural changes
Disinfection
Water systems
Temperature shock

ABSTRACT

Temperature-based strategies are commonly applied to control microbial growth, but the impact of those procedures on biofilm structure is usually not evaluated. This study investigates how thermal disinfection procedures affect pre-established *Pseudomonas fluorescens* biofilms, formed in a Center for Disease Control (CDC) biofilm reactor. It also assesses the biofilm regrowth potential over 24 h, under 125 and 225 rpm. Biofilms structure was compared at the mesoscale (thickness) and at the microscale (biovolume and surface coverage). Results showed that the impact of the thermal disinfection on the biofilm structure depends on the hydrodynamic conditions, which are also critical to the biofilm structural rearrangement upon regrowth. A thickness reduction of 80 % was found after the shock for biofilms formed under 125 rpm, however there was no significant biofilm sloughing off for the 225 rpm. Surface coverage was reduced by 65 % and 6 % after the thermal shock for 125 and 225 rpm, respectively. Furthermore, results seem to indicate that regardless the biofilm structural characteristics, bacteria recovered their culturability and viability to similar values to the ones before the thermal shock. This work provides an initial framework to develop more sustainable and effective thermal disinfection procedures in engineered water networks.

1. Introduction

Thermal disinfection (or heat sanitization) approaches are widely applied to control microorganisms' growth [1]. Increasing the water temperature, above the operating temperature for a certain period (the shock period), is known to decrease the number of microorganisms in suspension [2]. In engineered water systems it can be used to minimize the incidence of waterborne pathogens like *Legionella* [3–6] or *Pseudomonas aeruginosa* [5,7,8]. Each specific aim of the thermal disinfection requires different temperatures, different shock periods and adjusted periodicities.

Real-field studies have been performed to evaluate thermal disinfection effectiveness [3,9,10]. For example, thermal disinfection efficacy was evaluated at 33 hot water distribution systems colonized by *Legionella* [3]. The temperature at the water storage tank was set to 70–80 °C, with water circulation through the system for up to 3 days, ensuring at least 65 °C at the end-points of the networks (e.g. taps). Results showed that, unless repeatedly implemented over time, thermal disinfection was not effective enough to eliminate pathogenic bacteria. The authors argue that *Legionella* prevalence after the thermal shock was most probably due to the protection conferred by biofilms.

Indeed, many temperature-time studies found in the literature target the impact of thermal treatment on the inactivation of planktonic microorganisms [11], too often ignoring the role of biofilms in shielding such microorganisms against external harsh conditions, including thermal shock [11,12]. But, the work of Farhat et al. (2010) [12] who compared the impact of a heat shock treatment (70 °C for 30 min) in *Legionella* populations in water and in biofilms showed that the heat shock did not completely destroy the biofilm, which rapidly increased in cell density. Similarly, Wahlen et al. (2016) [13] studied the inactivation kinetics of *Sphingomonas parapaucimobilis* in planktonic and sessile states at temperatures ranging from 65 to 80 °C, and observed greater resistance of the biofilm (lower cell culturability reductions) to the hot water when compared with the planktonic cells.

From the operational point-of-view of engineered water networks, it is important to assess what happens to the bacterial cells and to the

* Corresponding author at: LEPABE - Laboratory for Process Engineering, Environment, Biotechnology and Energy, Faculty of Engineering, University of Porto, Rua Dr. Roberto Frias, 4200-465 Porto, Portugal.
E-mail address: aalex@fe.up.pt (A. Pereira).

https://doi.org/10.1016/j.jwpe.2023.103595
Received 18 November 2022; Received in revised form 16 February 2023; Accepted 17 February 2023
Available online 3 March 2023

biofilm structure upon thermal disinfection. The biofilm structure is intrinsically linked to the effect of hydrodynamics on mass transfer [14,15], and will ultimately affect the detachment rates [16].

Understanding what happens to the biofilm structure after a thermal shock and whether the thermal effect is similar or not under different flow velocities can provide important contributions to designing and implementing better thermal procedures. The present work addresses these two points, evaluating the biofilm structural parameters with microscale (Confocal Laser Scanning Microscopy, CLSM) and mesoscale imaging (Optical Coherence Tomography, OCT). For that, *Pseudomonas fluorescens* biofilms were formed in a Center for Disease Control (CDC) biofilm reactor for 8 days.

The biofilm was subjected to thermal shocks (70 °C over 15 min) and coupons were sampled prior to the shock and post-shock after 1 and 24 h. The biofilm micro- and mesoscale changes and the regrowth potential after the shock were evaluated under two turbulent flow stirring velocities (125 and 225 rpm). Additionally, biofilm culturability (by colony-forming unit (CFU) counts) and viability (by Adenosine Triphosphate (ATP) bioluminescence assay) were also determined. To the best of the authors' knowledge, this is the first study that assesses the impact of a temperature shock on biofilms structure at the micro- and mesoscale under different shear stress conditions. This paper describes a proof-of-concept undertaken in a reproducible and standardized biofilm model to investigate and validate the role of biofilm structure on thermal disinfection efficacy.

2. Material and methods

2.1. Bacteria culture and growth media

The bacterial strain used to form biofilm was *Pseudomonas fluorescens* ATCC 13525^T, obtained from the American Type Culture Collection. *Pseudomonas fluorescens* is a well-studied Gram-negative bacterium, a good biofilm producer and commonly used as a model bacterium in several biofilm studies [17–20]. It is a frequent inhabitant of freshwater environments and one of the first colonizers of water supply networks [21]. Multispecies biofilms are more complex than monospecies ones and provide a more realistic representation of what happens in real-field water systems [22], while monospecies biofilm models can offer simplicity, standardization and a good reproducibility [23]. Besides, *P. fluorescens* is often found in water samples along with waterborne pathogens, such as *Legionella pneumophila* [24]. Overnight cultures were grown at 30 ± 3 °C under agitation (120 rpm) in 100 mL of a sterile nutrient medium. This medium consisted of, per liter, 5.5 g glucose, 2.5 g peptone, 1.25 g yeast extract in phosphate buffer (1.88 KH_2PO_4 and 2.6 $NaHPO_4$). All components were purchased from Merck (Darmstadt, Germany).

2.2. Biofilm formation

The CDC Biofilm Reactor (Biosurface Technologies, USA) was used for biofilm formation. This platform is a standardized device commonly used as a drinking water system model [25–28], and it was designed to have the characteristics of a biofilm grown under moderate to high fluid shear [29]. This device consists of a 1-liter glass beaker with 8 polypropylene rods suspended from a ported lid (https://biofilm.montana.edu/standardized-biofilm-methods-training-videos.html) [29]. Each rod accommodates 3 circular polyvinyl chloride (PVC) coupons with 1.27 cm diameter (Neves & Neves, Portugal), that are positioned perpendicularly to a rotating baffle. Polyvinyl chloride (PVC) was selected since it is commonly found in residential plumbing [30,31].

Coupons were cleaned according to the ASTM E2871 [32]. Briefly, coupons were sonicated in a 10 % sodium dodecyl sulphate (VWR International, Portugal) solution for 5 min. To remove any remaining detergent, coupons were rinsed with tap water and then sonicated again in ultrapure water. Afterwards, coupons were rinsed in ultrapure water, air dried, and sterilized with ultraviolet (UV) radiation for 30 min. Meanwhile, the CDC biofilm reactor was sterilized, and the coupons were placed in the rods aseptically.

On day 0, the bioreactor was inoculated with 1 mL of the overnight culture (10^8 CFU/mL *P. fluorescens*) in 500 mL of sterile nutrient medium. The baffle was set to rotate at either (a) 125 (0.0205 N/m^2) or (b) 225 (0.0573 N/m^2) rpm [33].

The bioreactor ran in batch mode for 24 h at room temperature. Afterwards, continuous flow for a total period of 10 days was initiated with 1:100 nutrient broth medium at 10 ± 0.5 mL/min.

2.3. Thermal shock treatment

Biofilm was formed for 8 days and a rod was aseptically removed to characterize the biofilm (prior to thermal shock). Then, the reactors bulk suspension was replaced by sterile nutrient medium (1:100 dilution) at 70 °C, which was maintained for 15 min, under the specified stirring velocity. The temperature remained constant throughout the 15 min period by turning on the heating plate. After that, the bulk phase was removed again and replaced by new diluted media at room temperature. Reactor holders were removed 1 and 24 h after the thermal shock for biofilm analysis.

The three major steps of this study are: (i) biofilm formation for 8-days at room temperature (temperature of the suspension: 25 °C), (ii) thermal shock treatment, 70 °C for 15 min, and (iii) biofilm regrowth at room temperature after thermal shock for 24 h. Flow conditions have been kept constant in all the steps.

Preliminary experiments (available as Supplementary data) showed that the biofilm log-density reached a plateau 4 days after starting biofilm formation. Other former studies also relied on 8-days-old biofilm models [1,21].

2.4. Biofilm analysis

2.4.1. Optical Coherence Tomography (OCT)

Biofilms were imaged using a spectral-domain Optical Coherence Tomography (OCT) using a Thorlabs Ganymede instrument (Thorlabs GmbH, Germany) with a central wavelength of 930 nm. The visualization field was 3.66 × 2.98 mm at the X-Z section, corresponding to 1024 × 1024 pixels. The refractive index was set to 1.40 to be similar to the refractive index of water (1.33), since biofilms are mainly composed of water [34]. Each coupon was placed inside a sterile 12-well microtiter plate (VWR International, Portugal) and each well was filled with 3 mL of a sterile saline solution (8.5 g/L NaCl, VWR International, Belgium) and imaged. For each coupon, 2D imaging was performed with a minimum of five different fields of view to ensure the accuracy and reproducibility of the results.

The acquired images were analyzed with the novel freeware software BISCAP (Biofilm Imaging and Structure Classification Automatic Processor), available at https://github.com/diogonarciso/BISCAP. This software requires minimal user input and the full details of the underlying image processing strategy are described in Narciso et al. [35]. In brief, firstly all pixels at the substratum are identified, exploring the fact that these are usually very bright. Then, a threshold intensity is calculated and all pixels binarized accordingly (biomass vs. background). At last, using 2 complementary pixel continuity checks, the full biofilm structure, and all pixels at the boundary with the liquid bulk are identified. All steps are fully automatic, except for thresholding where the threshold intensity may be manually set if required. BISCAP delivers multiple image outputs for detailed biofilm visualization and analysis. It also delivers a set of common biofilm structural parameters, including average thickness.

The mean biofilm thickness can be calculated as the length between the interfaces (top and bottom) that delineates the biofilm structure [35], from the 2D-OCT images.

2.4.2. Confocal Laser Scanning Microscopy

Biofilm samples were stained with 5 μM SYTO® 61 (Invitrogen Life Technologies, Alfagene, Portugal), a cell-permeant fluorescent nucleic acid marker, and observed with a helium-neon laser at an excitation wavelength of 633 nm and using a 40× water objective lens (Leica HC PL APO CS, Leica Microsystems, Germany) in an inverted microscope Leica DMI6000-CS. A minimum of six stacks of horizontal plane images (512 × 512 pixels, corresponding to 387.5 × 387.5 μm) with a z-step of 1 μm were acquired for each sample. Three-dimensional (3D) projections of biofilm structures were constructed from the CLSM image acquisitions using the "Easy 3D" tool of IMARIS 9.1 software (Bitplane, Switzerland). Additionally, the plug-in COMSTAT2 associated with the ImageJ software was used to quantify the biovolume ($\mu m^3/\mu m^2$) and surface coverage (%) [36]. The biovolume was defined as the volume of biomass (μm^3) from a certain biofilm area divided by the surface area of the substratum (PVC coupons) (μm^2). The surface coverage (%), which is the fraction of the area occupied by biomass in the surface horizontal plane, reflects how efficiently the surface is colonized.

2.4.3. Culturability

The coupons taken from each rod were washed twice in sterile saline solution (8.5 g/L NaCl), and then aseptically transferred to 50 mL falcon tubes with 10 mL of saline solution for disaggregation. Each coupon was submitted to three alternate cycles of 30 s sonication (Ultrasonic Cleaner USC-T, 45 kHz, VWR International, Portugal), followed by 30 s of vortexing. Serial dilutions were performed and plated in triplicate in R_2A agar (Oxoid) for colony-forming units (CFU) enumeration.

2.4.4. ATP bioluminescence

To measure the adenosine triphosphate (ATP) released from the cells, the BacTiter-Glo™ Microbial Cell Viability Assay (Promega Corporation, USA) was used. This kit allows the determination of the number of viable bacterial cells in culture based on quantification of the ATP that is present in the sample. ATP is an indicator of metabolically active cells [37,38]. To measure ATP from bacteria, 100 μL of the bacterial suspension was mixed with 100 μL of BacTiter-Glo™ reagent (prepared according to manufacturer' instructions) on an opaque-walled multiwell plate. Control wells containing medium (saline solution or a bulk phase sample) were also prepared to obtain a value for background luminescence (negative control). Plate contents were mixed, incubated for 5 min, and read in a bioluminometer (FLUOstar Omega, BMG LABTECH, Germany). The output values are in relative light units per cm^2 (RLU/cm^2).

2.5. Statistical analysis

The experimental data were analyzed using the software GraphPad Prism 9.0 for Windows (GraphPad Software, USA). All measurements were performed in duplicate, and all experiments were performed in three independent replicates. The mean and standard deviation (SD) for each set of results were calculated. Differences between measurements were evaluated using an ANOVA single factor statistical analysis. The level of significance was set for p-values < 0.05.

3. Results

The effect of temperature shock (70 °C, 15 min) on the 8-days-old *Pseudomonas fluorescens* biofilms was accomplished by assessing, prior to and 1 h and 24 h after the shock: a) the biofilm structural changes (at the meso- and microscale); b) the microbiological indicators (culturability and ATP bioluminescence).

3.1. Thermal shock impact on biofilm mesoscale structure

The biofilm structure at the mesoscale was investigated before the thermal shock and 1 and 24 h after the thermal shock, using Optical Coherence Tomography (2D–OCT) imaging. The 2D-OCT biofilm images depicted in Fig. 1 suggest that different structures were observed for the biofilms formed at the two tested shear stresses (comparison between images before the thermal shock for 125 and 225 rpm). Furthermore, when comparing the immediate impact of the thermal shock on each of the biofilms it seems that the biofilms rearrange differently depending on such shear stress (comparison between Fig. 1a) and b)).

3.1.1. Thermal shock impact on biofilm thickness

The results for the 125 rpm biofilm (Fig. 2a) show that the thermal shock had a significant impact on the biofilm thickness reduction. Such reduction is up to 80 % when comparing the data before the shock (BS) - 108 ± 25 μm, and 1 h after the shock (1 h AS) - 20 ± 11 μm.

These results suggest that for 125 rpm grown biofilms, the thermal shock leads to immediate biofilm detachment, at least from the outer layers, which are probably less cohesive when compared to the basal layers. This phenomenon has been named by other researchers as 'stratification of the biofilm cohesion' [39]. It is interesting to note that 24 h after the shock (24h_AS), the biofilm thickness increased as compared to 1 h after the shock (1h_AS), but to values significantly lower than the ones observed before the shock.

Considering the thickness results observed for the biofilms formed at the higher rotational speed (225 rpm, Fig. 2b), no significant impact of the thermal shock on the biofilm thickness was observed. Indeed, thickness was similar before (BS) and 1 h after the shock ($p > 0.05$), with an average value of 66 ± 17 μm.

When comparing the effect of shear stress on biofilm formation (Fig. 2), the biofilms formed at 125 rpm (BS_125 rpm) (108 ± 25 μm) were thicker than the ones formed at 225 rpm (BS_225 rpm) (64 ± 20 μm). These thickness values were found to be statistically different ($p < 0.0001$).

3.2. Thermal shock impact on biofilm microscale structure

To further evaluate the effect of a thermal shock on mature *P. fluorescens* biofilms, their microstructure was examined by Confocal Laser Scanning Microscopy (CLSM) before shock (BS), and 1 (1h AS) and 24 (24h AS) hours after shock. The 8-days-old biofilms formed under both hydrodynamic conditions and before the temperature shock were very dense. However, the biofilm grown at 125 rpm was thicker than the biofilm formed at 225 rpm, as previously observed by OCT (Figs. 1 and 2). This lower thickness of biofilms formed at higher shear stress is in agreement with the lower biovolume of this biofilm when compared to the biofilm formed at 125 rpm (about 55 % less; Fig. 4a, b). Regarding the biofilm regrowth behavior after the heat treatment, the differences in biofilm structure between 125 and 225 rpm are evident. There was a drastic reduction in the biomass of the biofilm formed at 125 rpm (Fig. 3a), such that after 1 h of exposure to fresh culture medium, the surface coverage of the biofilm was only 29 % (as opposed to 83 % of biofilm surface coverage before T-shock) and the biovolume of 18 $\mu m^3/\mu m^2$ (as opposed to 80 $\mu m^3/\mu m^2$ determined before T-shock) ($p < 0.0001$; Fig. 4a, c). Indeed, the representative image of biofilm 1 h after T-shock (Fig. 3a, second line) shows a thinner biofilm arrangement and isolated bacterial colonies heterogeneously distributed on the surface. The effect of heat treatment was not as aggressive on the biofilm formed at 225 rpm, where after 1 h the biovolume and surface coverage reduced by 6 % ($p > 0.05$) and 23 % ($p < 0.0001$), respectively (Fig. 4b, d). When the regrowth time was extended to 24 h, the biofilm under 125 rpm had a thicker and denser structure (Fig. 3a, third line), reaching a biovolume of 34 $\mu m^3/\mu m^2$ ($p < 0.0001$) and surface coverage of 76 % ($p < 0.05$; Fig. 4a, c), similar to that obtained before the T-shock. In the case of biofilms exposed to 225 rpm, 24 h after the T-shock, the biovolume remained similar to that determined for the control sample (BS) and the biofilm 1 h after T-shock ($p > 0.05$), but the surface coverage suffered a gradual decrease, attaining 59 % (Fig. 4b, d).

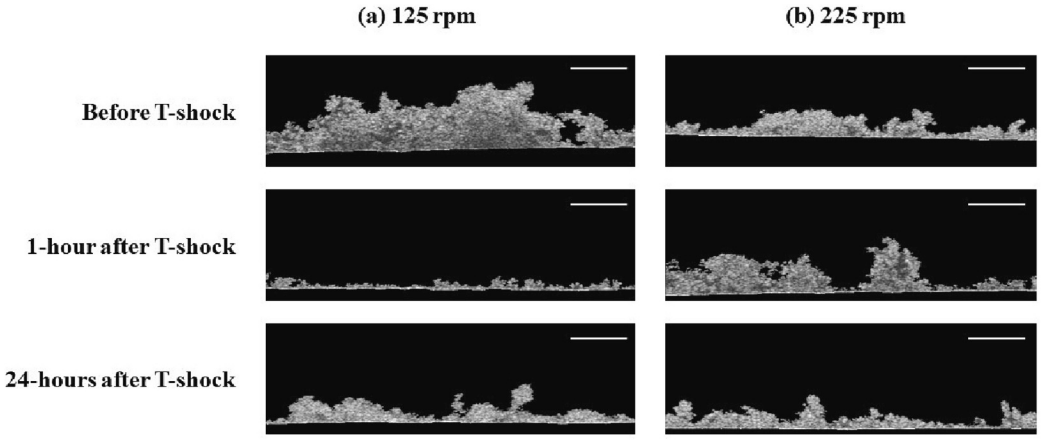

Fig. 1. Representative images obtained by Optical Coherence Tomography (OCT) of 8-day-old biofilms developed under (a) 125 and (b) 225 rpm before the thermal shock, and 1 and 24 hours after thermal shock (T-shock). White scale bars are 100 μm. These images were obtained using BISCAP software and show biofilm vertical stacks.

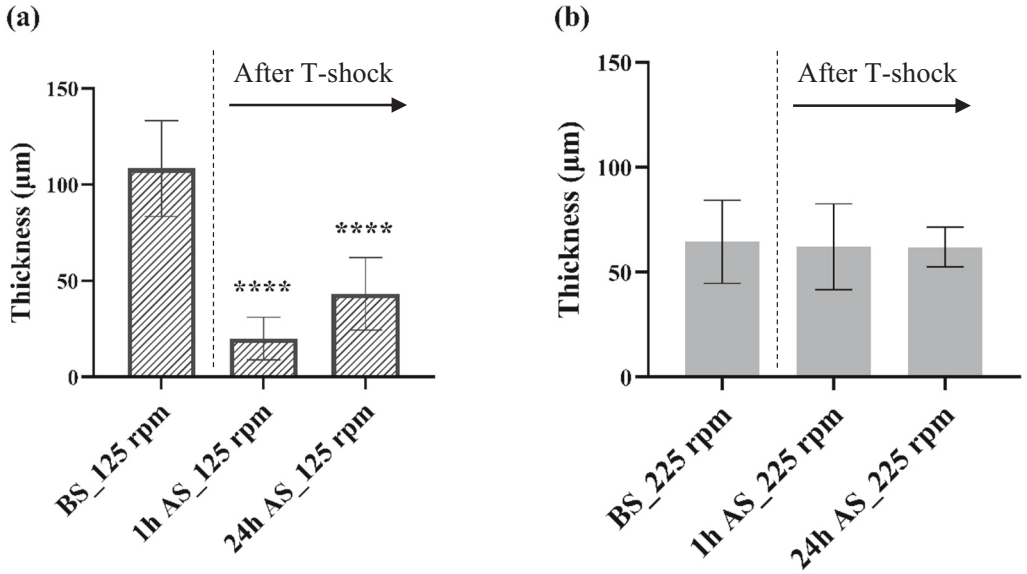

Fig. 2. Thickness of 8-day-old biofilms developed under 125 rpm (a) and 225 rpm (b), before shock (BS) and 1 (1h AS) and 24 (24h AS) hours after shock (AS). The data present the mean ± standard deviation (SD) of three independent experiments. Statistically significant differences are represented for <0.0001 by **** when compared with BS samples.

3.3. Culturability

The $\log_{10}$ colony-forming units per cm^2 (CFU/cm^2) of biofilm cells over time (before and 1 and 24 h after the thermal shock) is shown in Fig. 5. Biofilms formed under 125 rpm had 10^8 CFU/cm^2 before the thermal shock (biofilm age of 8-days). In Fig. 5a, it was possible to observe the reduction of colony forming units per cm^2 (a 4-$\log_{10}$ reduction was achieved) 1 h after the shock, which demonstrates the effectiveness of the thermal treatment on cell culturability reduction.

Regarding the post-shock period (24 h), thermally treated biofilms showed a high culturability increase during the first 24 h after the thermal shock, so the biofilms seemed to have recovered and reached their previous population *plateau* (8.01×10^7 CFU/cm^2).

Regarding the 225 rpm grown biofilms, the culturability values before and after (1 and 24 h) thermal shock were similar to those obtained for biofilms grown under 125 rpm ($p > 0.05$; Fig. 5b).

3.4. Viability

To investigate the metabolic activity of *P. fluorescens* cells in the biofilm, ATP was quantified. Fig. 6a shows the luminescence values that were recorded (in RLU/cm^2) for 125 rpm biofilms before and after (1 and 24 h) the thermal shock. The thermal shock had significantly reduced the ATP production (reduction of ~98 %; $p < 0.0001$) 1 h after the shock. This conclusion seems to agree with the fact that upon exposure to stress events, bacteria tend to significantly reduce their ATP levels [40].

In the present study (Fig. 6a), the ATP decrease was only observed in the sampling point of 1 h after the shock, as in the following time-point (24 h) cells recovered their viability to levels like the ones determined prior to the shock ($p > 0.05$).

Furthermore, when comparing these results with the ones from Fig. 6b, it can be seen that the viability of the cells in the biofilm formed at 225 rpm followed a similar trend as the one from 125 rpm. Indeed, the RLU/cm^2 values before and after thermal shock were all similar to those obtained for biofilms grown under 125 rpm ($p > 0.05$) issuing, as

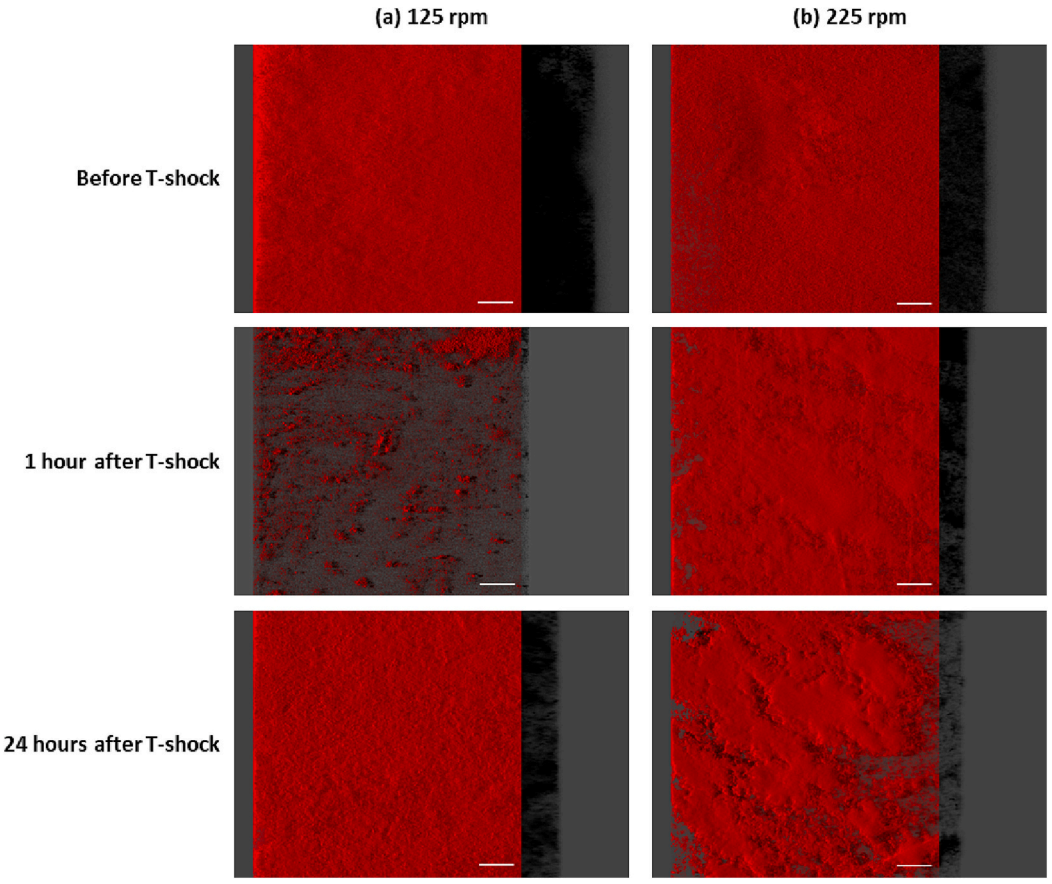

Fig. 3. Representative three-dimensional (3D) confocal images of *P. fluorescens* ATCC 13525^T biofilms developed under (a) 125 and (b) 225 rpm before the thermal shock, and 1 and 24 hours after thermal shock (T-shock). White scale bars are 50 μm. These images were obtained by IMARIS software and show the biofilm aerial view, with the virtual shadow projection on the right (illustrative of biofilm thickness).

expected, that the tested shear stress does not seem to affect the *P. fluorescens* viability within the biofilm, nor to promote different response after the thermal shock.

4. Discussion

The main results discussed so far, are summarized in Fig. 7.

4.1. The role of biofilm structure on temperature shock

4.1.1. Biofilm characteristics prior to the shock

Biofilms formed under the tested shear stress conditions were found to be structurally different in terms of: i) mesoscale properties (thickness) and ii) microscale properties (surface coverage and biovolume). As discussed, the biofilms formed at higher rotational speed (225 rpm) were found to be significantly thinner than those formed under 125 rpm. This is in accordance with former studies [41,42]. In fact, it is widely established across literature that hydrodynamics strongly affects biofilm structures [43], and ultimately the mass transfer processes [44,45]. For example, under higher fluid velocities, more nutrients and oxygen reach the biofilms surface [45], but diffusion inside the biofilm depends on its cohesiveness [46].

In the present study, regardless the structural differences already mentioned, the number of culturable cells and the ATP levels per area were comparable for both tested rotational speeds, respectively ~10^8 CFU/cm^2 and ~10^5 RLU/cm^2. Looking into the biofilm cell density (calculated by dividing CFU/cm^2 by the biofilm thickness), it becomes clear that although the total number of culturable cells per area was the same, the cell density was much lower for the thicker biofilm - the one formed at 125 rpm. This might be explained by the fact that under lower fluid velocities, a lower number of cells will be available to adhere to surfaces and colonize them, thus lower cell densities will be achieved [47].

4.1.2. Biofilm characteristics after the thermal shock

Similarly to what happens when biofilms are exposed to other stresses like flow increase or biocides [48,49], the biofilm structural characteristics seem to be key to what happens when the biofilms are thermally shocked. As shown in Fig. 7, the thermal shock has a significant impact on the biofilms formed at the lower velocity (125 rpm), due to biofilm detachment (sloughing off), corresponding to an 80 % decrease in thickness and biovolume after the stress event. This detachment was followed by a quick structural reorganization of the biofilm in terms of micro- and mesoscale into a thinner layer with a more homogeneous matrix. This reorganization was noticeable in terms of thickness, biovolume and surface coverage, 1 h after the shock and did not significantly change over the 24 h period (Fig. 7). Similarly, Chang et al. (2017) [50], reported that *Bacillus subtilis* biofilms became thinner with reduced volume and surface coverage, after thermal shocks under different temperatures and exposure times.

On the other hand, biofilms formed under higher rotational speed (225 rpm) were found to be more stable (less susceptible to slough-off caused by thermal shock) as no significant differences are observed in terms of mesoscale thickness over time. In fact, it is widely known that biofilms formed at higher shear stress conditions tend to be more resistant to external stresses (biocides, flow increase, etc.) [51,52]. For example, a former study demonstrated that *P. fluorescens* biofilms grown under higher shear stresses are more strongly adhered, have stronger

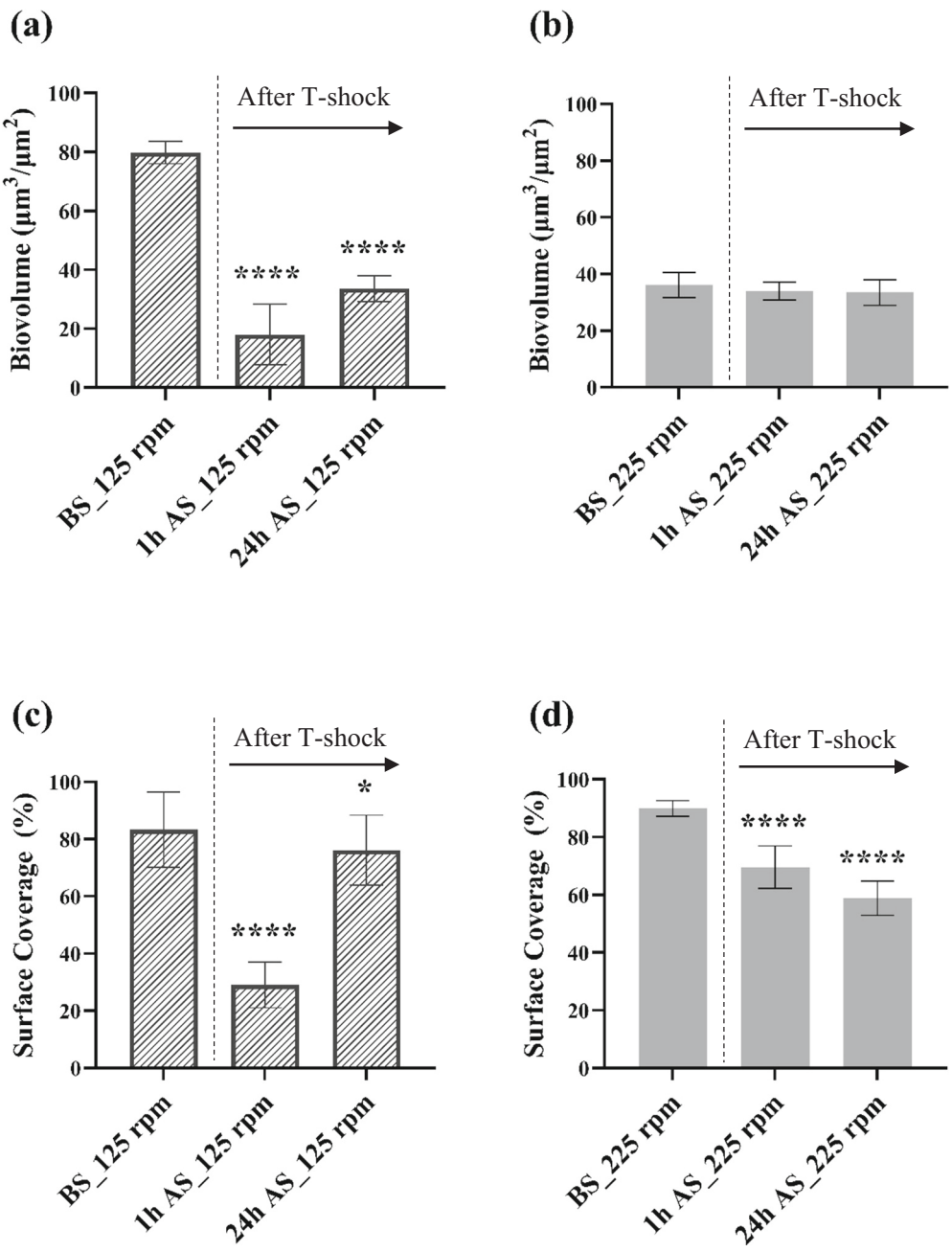

Fig. 4. Biovolume (a, b) and surface coverage (c, d) of 8-day-old biofilms developed under 125 rpm (a, c) and 225 rpm (b, d) before shock (BS) and 1 (1h AS) and 24 (24h AS) hours after shock (AS). Values were extracted from confocal files with the COMSTAT program. The means ± standard deviation are shown. Statistically significant differences are represented for $p < 0.05$ by * and <0.0001 by **** when compared with BS samples.

(more compact) EPS matrix and, thus, tend to be more stable upon unexpected stress events [41].

4.2. *Different impact of the thermal shocks on the biofilm structure versus cells' culturability and viability*

It is interesting to note that the thermal shocks have a different impact on the structure and on the microbiological features (culturability and viability) of the biofilm. For example, when considering the 225 rpm rotational velocity, even though thickness was similar prior and after the shock (1 and 24 h), there was a significant decrease in culturability and ATP levels 1 h after the thermal shock. Other authors also found that the application of chemical treatments could cause a significant reduction on biofilm cells' count even though biomass does not significantly decrease [53]. Then, in the 24 h after the shock these indicators increased to levels comparable to the ones prior to the thermal shock. A similar trend was observed for the lower stirring velocity. This data suggests that exposing *P. fluorescens* biofilms to 70 °C over 15 min 'endangered' the bacterial cells within the biofilm to an extent that was still found 1 h after the initial bulk conditions were restored (~25 °C). However, it seems that the thermal effect on the biofilm cells was very limited in time, as for both tested shear stresses, 24 h after the shock, culturability and viability (ATP) recovered to values like the ones observed in the biofilm before the shock. Former work from Ricker et al. (2018) [7] showed that above a 'critical post-shock bacterial loading' (of approximately 10^3 CFU/cm^2) of *Pseudomonas aeruginosa* biofilms thermally shocked can regrowth to their initial population density. Barros et al. (2022) [19] also showed that previously labelled 'dead'

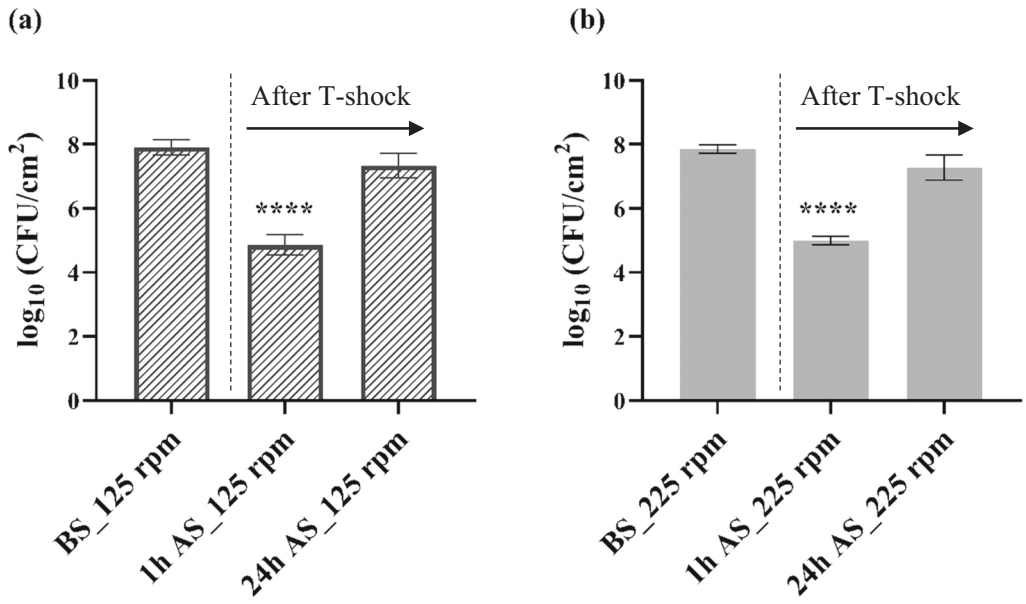

Fig. 5. Culturability of *P. fluorescens* biofilms developed under 125 (a) and 225 (b) rpm, before shock (BS) and 1 (1h AS) and 24 (24h AS) hours after shock (AS). The data present the mean ± standard deviation (SD) of three independent experiments. Statistically significant differences are represented for $p < 0.0001$ by **** when compared with BS samples.

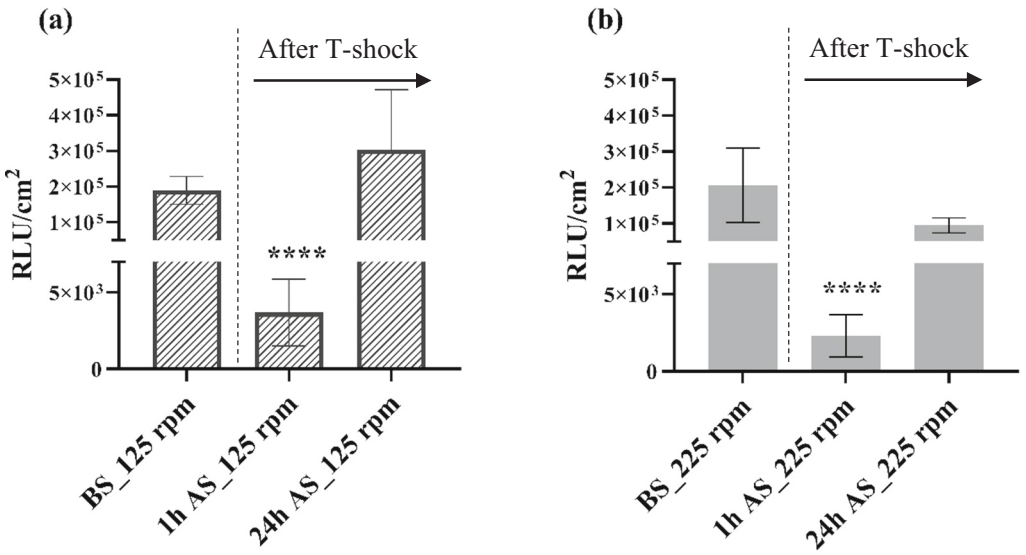

Fig. 6. Viability measured in RLU/cm^2 for *P. fluorescens* biofilms developed under 125 (a) and 225 (b) rpm, before shock (BS) and 1 (1h AS) and 24 (24h AS) hours after shock (AS). The data present the mean ± standard deviation (SD) of three independent experiments. Statistically significant differences are represented for $p < 0.0001$ by **** when compared with BS samples.

P. fluorescens cells after biodical exposure [18] are able to regain viability (increased ATP production) when optimum growth conditions are restored.

Other authors concluded that a heat shock (70 °C for 30 min) did not destroy a drinking water biofilm, that rapidly increased in log density [12]. Apart from the arguments already provided, the culturability and viability recovery after 24 h might also be related to: a) the fact that 1 h after the shock, the temperature inside the biofilm was still above the bulk temperature, thus promoting an 'inhibition' effect on the functional behavior of cells [54]; b) cells adhering to the PVC coupons might also attach to the reactor's walls (this was clearly observed), which might be responsible for a fast recolonization; c) high temperatures (80–90 °C) might have a 'baking' effect on the attached biofilms, increasing its adherence to the surface and enhancing a rapid recolonization [55]; d) dead biomass can be a source of nutrients, by promoting necrotrophic growth upon regrowth [1]. It is also worth noting that the shift in cell culturability and viability followed the same trend regardless of biofilm structural characteristics.

To design appropriate thermal disinfection procedures, an understanding about the fundamental impact of thermal shock on biofilm structure should be known. Using a reproducible biofilm model, assessed with a micro- and mesoscale analysis, this work provides new insights on the need of studying biofilm structure. Future studies should be performed with more complex biofilm models, different temperature and time conditions, and different pipe materials to better understand the points herein discussed.

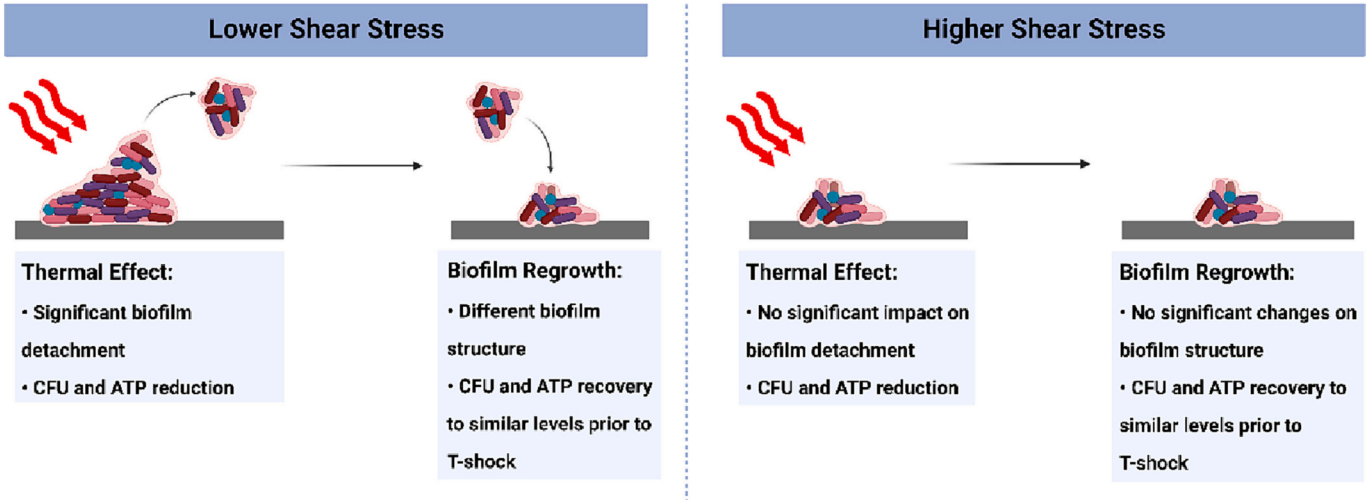

Fig. 7. Illustration of the impact of temperature shock (T-shock) on biofilm structure, culturability and viability.

5. Conclusions

Thermal disinfection procedures are widely used across engineered water systems to address microbiological control. This study, while combining micro- and mesoscale imaging of the biofilm with microbial culturability and viability, highlights important findings regarding the impact of thermal shocks on 8-days-old *Pseudomonas fluorescens* biofilms. Those findings are: a) the effect of thermal shock on the biofilm structure seems to depend on the prevailing hydrodynamic conditions; b) there is a different structural spatial arrangement of the biofilm after the thermal shock, and c) the thermal shock affects differently the biofilm structure and its cell culturability and viability.

CRediT authorship contribution statement

Conceptualization, A.R.S, L.F.M. and A.P.; supervision, L.F.M. and A.P.; writing—original draft, A.R.S. and A.P.; writing—review and editing, all authors; BISCAP software development, D.A.C.N. and F.G.M; CLSM analysis, L.C.G.; funding, L.F.M. All authors have read and agreed to the published version of the manuscript.

Declaration of competing interest

The authors declare that they have no known competing financial interests or personal relationships that could have appeared to influence the work reported in this paper.

Data availability

Data will be made available on request.

Acknowledgements

This work is financially supported by: LA/P/0045/2020 (ALiCE), UIDB/00511/2020 and UIDP/00511/2020 (LEPABE), funded by national funds through FCT/MCTES (PIDDAC). This work is also financially supported by national funds through the FCT/MCTES (PIDDAC), under the project 2022.03523.PTDC. Funding from the European Union—Horizon 2020 research and innovation program under grant agreement No 952471 (SurfSAFE). Project HealthyWaters (NORTE-01-0145-FEDER-000069), supported by Norte Portugal Regional Operational Programme (NORTE 2020), under the PORTUGAL 2020 Partnership Agreement, through the European Regional Development Fund (ERDF). Ana Rosa Silva thanks the Portuguese Foundation for Science and Technology (FCT) for the financial support of the PhD grant (2020.08539.BD).

Appendix A. Supplementary data

Supplementary data to this article can be found online at https://doi.org/10.1016/j.jwpe.2023.103595.

References

[1] A. Nocker, E. Lindfeld, J. Wingender, S. Schulte, M. Dumm, B. Bendinger, Thermal and chemical disinfection of water and biofilms: only a temporary effect in regard to the autochthonous bacteria, J. Water Health 19 (2021) 808–822, https://doi.org/10.2166/wh.2021.075.
[2] G. Cebrián, S. Condón, P. Mañas, Physiology of the inactivation of vegetative bacteria by thermal treatments: mode of action, influence of environmental factors and inactivation kinetics, Foods 6 (2017) 107, https://doi.org/10.3390/foods6120107.
[3] V. Mouchtouri, E. Velonakis, C. Hadjichristodoulou, Thermal disinfection of hotels, hospitals, and athletic venues hot water distribution systems contaminated by Legionella species, Am. J. Infect. Control 35 (2007) 623–627, https://doi.org/10.1016/j.ajic.2007.01.002.
[4] D.S. Blanc, P. Carrara, G. Zanetti, P. Francioli, Water disinfection with ozone, copper and silver ions, and temperature increase to control legionella: seven years of experience in a university teaching hospital, J. Hosp. Infect. 60 (2005) 69–72, https://doi.org/10.1016/j.jhin.2004.10.016.
[5] S. Yui, K. Karia, S. Ali, M. Muzslay, P. Wilson, Thermal disinfection at suboptimal temperature of Pseudomonas aeruginosa biofilm on copper pipe and shower hose materials, J. Hosp. Infect. 117 (2021) 103–110, https://doi.org/10.1016/j.jhin.2021.08.016.
[6] C. Zhang, K. Qin, I. Struewing, H. Buse, J. Santo Domingo, D. Lytle, J. Lu, The bacterial community diversity of bathroom hot tap water was significantly lower than that of cold tap and shower water, Front. Microbiol. 12 (2021), https://doi.org/10.3389/fmicb.2021.625324.
[7] E.B. Ricker, H.A.S. Aljaafari, T.M. Bader, B.S. Hundley, E. Nuxoll, Thermal shock susceptibility and regrowth of Pseudomonas aeruginosa biofilms, Int. J. Hyperth. 34 (2018) 168–176, https://doi.org/10.1080/02656736.2017.1347964.
[8] E.B. Ricker, E. Nuxoll, Synergistic effects of heat and antibiotics on Pseudomonas aeruginosa biofilms, Biofouling 33 (2017) 855–866, https://doi.org/10.1080/08927014.2017.1381688.
[9] L. Gavaldà, M. Garcia-Nuñez, S. Quero, C. Gutierrez-Milla, M. Sabrià, Role of hot water temperature and water system use on Legionella control in a tertiary hospital: an 8-year longitudinal study, Water Res. 149 (2019) 460–466, https://doi.org/10.1016/j.watres.2018.11.032.
[10] J.J. Molina, M. Bennassar, E. Palacio, S. Crespi, Low efficacy of periodical thermal shock for long-term control of Legionella spp. in hot water system of hotels, Pathogens 11 (2022), https://doi.org/10.3390/pathogens11020152.
[11] A. Pereira, A.R. Silva, L.F. Melo, Legionella and biofilms—integrated surveillance to bridge science and real-field demands, Microorganisms 9 (2021), https://doi.org/10.3390/microorganisms9061212.
[12] M. Farhat, M.C. Trouilhé, E. Briand, M. Moletta-Denat, E. Robine, J. Frère, Development of a pilot-scale 1 for Legionella elimination in biofilm in hot water network: heat shock treatment evaluation, J. Appl. Microbiol. 108 (2010) 1073–1082, https://doi.org/10.1111/j.1365-2672.2009.04541.x.
[13] L. Wahlen, A. Parker, D. Walker, M. Pasmore, P. Sturman, Predictive modeling for hot water inactivation of planktonic and biofilm-associated Sphingomonas

parapaucimobilis to support hot water sanitization programs, Biofouling 32 (2016) 751–761, https://doi.org/10.1080/08927014.2016.1192155.
[14] M. Vieira, L. Melo, M. Pinheiro, Biofilm formation: hydrodynamic effects on internal diffusion and structure, Biofouling 7 (1993) 67–80, https://doi.org/10.1080/08927019309386244.
[15] Z. Lewandowski, H. Beyenal. Fundamentals of Biofilm Research, Second Edition, 2013, https://doi.org/10.1201/b16291.
[16] P. Stoodley, Z. Lewandowski, J.D. Boyle, H.M. Lappin-Scott, Structural deformation of bacterial biofilms caused by short-term fluctuations in fluid shear: an in situ investigation of biofilm rheology, Biotechnol. Bioeng. 65 (1999) 83–92. PMID: 10440674.
[17] C. Ferreira, R. Rosmaninho, M. Simoes, M.C. Pereira, M.M.S.M. Bastos, O.C. Nunes, M. Coelho, L.F. Melo, Biofouling control using microparticles carrying a biocide, Biofouling 26 (2010) 205–212, https://doi.org/10.1080/08927010903419630.
[18] A.C. Barros, L.F. Melo, A. Pereira, A multi-purpose approach to the mechanisms of action of two biocides (benzalkonium chloride and dibromonitrilopropionamide): discussion of Pseudomonas fluorescens' viability and death, Front. Microbiol. 13 (2022), https://doi.org/10.3389/fmicb.2022.842414.
[19] A.C. Barros, L.F. Melo, A. Pereira, Pseudomonas fluorescens cells' recovery after exposure to BAC and DBNPA biocides, Antibiotics 11 (2022), https://doi.org/10.3390/antibiotics11081042.
[20] S. Fernandes, I.B. Gomes, S.F. Sousa, M. Simões, Antimicrobial susceptibility of persister biofilm cells of Bacillus cereus and Pseudomonas fluorescens, Microorganisms 10 (2022), https://doi.org/10.3390/microorganisms10010160.
[21] M.S. Zekanović, G. Begić, S. Mežnarić, I. Jelovica Badovinac, R. Krištof, D. Tomić Linšak, I. Gobin, Effect of UV light and sodium hypochlorite on formation and destruction of Pseudomonas fluorescens biofilm in vitro, Processes 10 (2022), https://doi.org/10.3390/pr10101901.
[22] M. Burmølle, D. Ren, T. Bjarnsholt, S.J. Sørensen, Interactions in multispecies biofilms: do they actually matter? Trends Microbiol. 22 (2014) 84–91, https://doi.org/10.1016/j.tim.2013.12.004.
[23] R.C.D. Swimberghe, T. Coenye, R.J.G. De Moor, M.A. Meire, Biofilm model systems for root canal disinfection: a literature review, Int. Endod. J. 52 (2019) 604–628, https://doi.org/10.1111/iej.13050.
[24] C.R. Stewart, V. Muthye, N.P. Cianciotto, Legionella pneumophila persists within biofilms formed by Klebsiella pneumoniae, Flavobacterium sp., and Pseudomonas fluorescens under dynamic flow conditions, PLoS One 7 (2012), e50560, https://doi.org/10.1371/journal.pone.0050560.
[25] C.R. Armbruster, T.S. Forster, R.M. Donlan, H.A. O'Connell, A.M. Shams, M. M. Williams, A biofilm model developed to investigate survival and disinfection of Mycobacterium mucogenicum in potable water, Biofouling 28 (2012) 1129–1139, https://doi.org/10.1080/08927014.2012.735231.
[26] J. Lu, H.Y. Buse, V. Gomez-Alvarez, I. Struewing, J. Santo Domingo, N.J. Ashbolt, Impact of drinking water conditions and copper materials on downstream biofilm microbial communities and Legionella pneumophila colonization, J. Appl. Microbiol. 117 (2014) 905–918, https://doi.org/10.1111/jam.12578.
[27] K.J. Szwetkowski, J.O. Falkinham, Methylobacterium spp. as emerging opportunistic premise plumbing pathogens, Pathogens 9 (2020), https://doi.org/10.3390/pathogens9020149.
[28] M.S. Spencer, A.C. Cullom, W.J. Rhoads, A. Pruden, M.A. Edwards, Replicable simulation of distal hot water premise plumbing using convectively-mixed pipe reactors, PLoS One 15 (2020), e0238385, https://doi.org/10.1371/journal.pone.0238385.
[29] E. Johnson, T. Petersen, D.M. Goeres, Characterizing the shearing stresses within the CDC biofilm reactor using computational fluid dynamics, Microorganisms 9 (2021) 1709, https://doi.org/10.3390/microorganisms9081709.
[30] J.A. McBain, B.R. G., C.C. E., C. Duane, L.R. G., R.A. H., S.S. A., G. Peter, Microbial characterization of biofilms in domestic drains and the establishment of stable biofilm microcosms, Appl. Environ. Microbiol. 69 (2003) 177–185, https://doi.org/10.1128/AEM.69.1.177-185.2003.
[31] A.A. Morvay, M. Decun, M. Scurtu, C. Sala, A. Morar, M. Sarandan, Biofilm formation on materials commonly used in household drinking water systems, Water Supply 11 (2011) 252–257, https://doi.org/10.2166/ws.2011.053.
[32] A. International, ASTM E2871-13 Standard Test Method for Evaluating Disinfectant Efficacy Against Pseudomonas Aeruginosa Biofilm Grown in CDC Biofilm Reactor Using Single Tube Method, 2013.
[33] D.M. Goeres, L.R. Loetterle, M.A. Hamilton, R. Murga, D.W. Kirby, R.M. Donlan, Statistical assessment of a laboratory method for growing biofilms, Microbiology 151 (2005) 757–762, https://doi.org/10.1099/mic.0.27709-0.
[34] M.J. Romeu, P. Alves, J. Morais, J.M. Miranda, E.D. de Jong, J. Sjollema, V. Ramos, V. Vasconcelos, F.J.M. Mergulhão, Biofilm formation behaviour of marine filamentous cyanobacterial strains in controlled hydrodynamic conditions, Environ. Microbiol. 21 (2019) 4411–4424, https://doi.org/10.1111/1462-2920.14807.
[35] D.A.C. Narciso, A. Pereira, N.O. Dias, L.F. Melo, F.G. Martins, Characterization of biofilm structure and properties via processing of 2D optical coherence tomography images in BISCAP, Bioinformatics 38-6 (2022) 1708–1715, https://doi.org/10.1093/bioinformatics/btac002.
[36] A. Heydorn, A.T. Nielsen, M. Hentzer, C. Sternberg, M. Givskov, B.K. Ersbøll, S. Molin, Quantification of biofilm structures by the novel computer program COMSTAT, Microbiology 146 (Pt 1) (2000) 2395–2407, https://doi.org/10.1099/00221287-146-10-2395.
[37] P.-J. Raugel, Promega, in: Rapid Food Anal. Hyg. Monit, Springer, 1999, pp. 456–467.
[38] S. Duda, J.L. Baron, M.M. Wagener, R.D. Vidic, J.E. Stout, Lack of correlation between Legionella colonization and microbial population quantification using heterotrophic plate count and adenosine triphosphate bioluminescence measurement, Environ. Monit. Assess. 187 (2015), https://doi.org/10.1007/s10661-015-4612-5.
[39] A. Rochex, A. Massé, R. Escudié, J.-J. Godon, N. Bernet, Influence of abrasion on biofilm detachment: evidence for stratification of the biofilm, J. Ind. Microbiol. Biotechnol. 36 (2009) 467–470, https://doi.org/10.1007/s10295-009-0543-x.
[40] C. Robben, A.K. Witte, D. Schoder, B. Stessl, P. Rossmanith, P. Mester, A fast and easy ATP-based approach enables MIC testing for non-resuscitating VBNC pathogens, Front. Microbiol. 10 (2019) 1365, https://doi.org/10.3389/fmicb.2019.01365.
[41] M. Pereira, M. Kuehn, S. Wuertz, T. Neu, L.F. Melo, Effect of flow regime on the architecture of a Pseudomonas fluorescens biofilm, Biotechnol. Bioeng. 78 (2002) 164–171, https://doi.org/10.1002/bit.10189.
[42] J.S. Teodósio, F.C. Silva, J.M.R. Moreira, M. Simões, L.F. Melo, M.A. Alves, F. J. Mergulhão, Flow cells as quasi-ideal systems for biofouling simulation of industrial piping systems, Biofouling 29 (2013) 953–966, https://doi.org/10.1080/08927014.2013.821467.
[43] Y. Shen, G.L. Monroy, N. Derlon, D. Janjaroen, C. Huang, E. Morgenroth, S. A. Boppart, N.J. Ashbolt, W.-T. Liu, T.H. Nguyen, Role of biofilm roughness and hydrodynamic conditions in Legionella pneumophila adhesion to and detachment from simulated drinking water biofilms, Environ. Sci. Technol. 49 (2015) 4274–4282, https://doi.org/10.1021/es505842v.
[44] E. Tsagkari, W.T. Sloan, Turbulence accelerates the growth of drinking water biofilms, Bioprocess Biosyst. Eng. 41 (2018) 757–770, https://doi.org/10.1007/s00449-018-1909-0.
[45] A. Soares, L.C. Gomes, G.A. Monteiro, F.J. Mergulhão, Hydrodynamic effects on biofilm development and recombinant protein expression, Microorganisms 10 (2022), https://doi.org/10.3390/microorganisms10050931.
[46] L. Melo, Biofilm physical structure, internal diffusivity and tortuosity, Water Sci. Technol. 52 (2005), https://doi.org/10.2166/wst.2005.0184.
[47] P. Araújo, M. Joana, M. Idalina, M. Filipe, M. Luís, S. Manuel, Influence of flow velocity on the characteristics of Pseudomonas fluorescens biofilms, J. Environ. Eng. 142 (2016), 4016031, https://doi.org/10.1061/(ASCE)EE.1943-7870.0001068.
[48] S. Bas, M. Kramer, D. Stopar, Biofilm surface density determines biocide effectiveness, Front. Microbiol. 8 (2017) 2443, https://doi.org/10.3389/fmicb.2017.02443.
[49] S. Salgar-Chaparro, L. Katerina, P. Thunyaluk, D. Adam, M.L. L., S.A.J. M., Nutrient level determines biofilm characteristics and subsequent impact on microbial corrosion and biocide effectiveness, Appl. Environ. Microbiol. 86 (2022), e02885-19, https://doi.org/10.1128/AEM.02885-19.
[50] S. Chang, J. Chen, L. Shi, Using thermal shock to inhibit biofilm formation in the treated sewage source heat pump systems, Appl. Sci. 7 (2017), https://doi.org/10.3390/app7040343.
[51] L.C. Simões, I.B. Gomes, H. Sousa, A. Borges, M. Simões, Biofilm formation under high shear stress increases resilience to chemical and mechanical challenges, Biofouling 38 (2022) 1–12, https://doi.org/10.1080/08927014.2021.2006189.
[52] C. Cunault, C. Faille, A. Calabozo-Delgado, T. Benezech, Structure and resistance to mechanical stress and enzymatic cleaning of Pseudomonas fluorescens biofilms formed in fresh-cut ready to eat washing tanks, J. Food Eng. 262 (2019) 154–161, https://doi.org/10.1016/j.jfoodeng.2019.06.006.
[53] X. Chen, P.S. Stewart, Biofilm removal caused by chemical treatments, Water Res. 34 (2000) 4229–4233, https://doi.org/10.1016/S0043-1354(00)00187-1.
[54] I. Pinel, R. Biškauskaitė, E. Pal'ová, H. Vrouwenvelder, M. van Loosdrecht, Assessment of the impact of temperature on biofilm composition with a laboratory heat exchanger module, Microorganisms 9 (2021), https://doi.org/10.3390/microorganisms9061185.
[55] K. Marion-Ferey, M. Pasmore, P. Stoodley, S. Wilson, G.P. Husson, J.W. Costerton, Biofilm removal from silicone tubing: an assessment of the efficacy of dialysis machine decontamination procedures using an in vitro model, J. Hosp. Infect. 53 (2003) 64–71, https://doi.org/10.1053/jhin.2002.1320.